CCFE
CULHAM CENTRE FOR FUSION ENERGY

UK Atomic Energy Authority

UKAEA-CCFE-PR(22)43

Andrew M. Alvarado, Hi Vo Tin, Jan S. Wr´obel,
Damian Sobieraj, Duc Nguyen-Manh, Saryu Jindal
Fensin, Enrique Martinez, Osman El-Atwani

Thermodynamic Study of Hf Addition to Refractory Low-Activation W-Ta-Cr-V High Entropy Alloy from First-Principles

Thermodynamic Study of Hf Addition to Refractory Low-Activation W-Ta-Cr-V High Entropy Alloy from First-Principles

Andrew M. Alvarado, Hi Vo Tin, Jan S. Wr´obel, Damian Sobieraj, Duc Nguyen-Manh, Saryu Jindal Fensin, Enrique Martinez, Osman El-Atwani

This is a preprint of a paper submitted for publication in Journal of Materials Research

Thermodynamic Study of Hf Addition to Refractory Low-Activation W-Ta-Cr-V High Entropy Alloy from First-Principles

Andrew M. Alvarado[a,b], Hi Vo Tin[c], Jan S. Wróbel[d], Damian Sobieraj[d], Duc Nguyen-Manh[e,f], Saryu Jindal Fensin[c], Enrique Martinez[b,g,*], and Osman El-Atwani[c,*]

[a]Theoretical Division, Los Alamos National Laboratory, Los Alamos, NM, USA [b]Department of Materials Science and Engineering, Clemson University, Clemson, South Carolina 29623 USA [c]Material Science and Technology Division Los Alamos National Laboratory, Los Alamos, NM, USA [d]Faculty of Materials Science and Engineering, Warsaw University of Technology, ul. Wołoska 141, 02-507 Warsaw, Poland [e]CCFE, United Kingdom Atomic Energy Authority, Abingdon OX14 3DB, UK [f]Department of Materials, University of Oxford, Oxford OX1 3PH, UK [g]Department of Mechanical Engineering, Clemson University, Clemson, South Carolina 29623, USA.

ARTICLE HISTORY
Compiled June 29, 2022

ABSTRACT
We present a Density Functional Theory-based cluster expansion model to predict the configurational energy of a multicomponent W-Ta-Cr-V-Hf quinary alloy. Coupled with Monte Carlo simulations we show that the model reproduces experimental observations. We analyze the thermodynamic properties of the $W_{.31}Ta_{.34}Cr_{.05}V_{.27}Hf_{.03}$ system and observe two phase transitions, one order-disorder transition at 1250 K from fully random to separation and a second one at 620 K from separation to ordering.

Impact Statement
Small amounts of Hf modify the equilibrium phases of the refractory W-Ta-Cr-V HEA at low temperatures, with both experiments and modeling agreeing on the correlations between different elements.

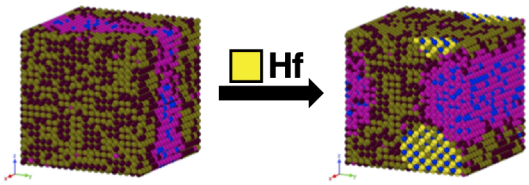

KEYWORDS
Cluster Expansion; refractory low-activation High Entropy Alloy; Hafnium Multicomponent; Density Functional Theory; Monte Carlo.

1. Introduction

High entropy alloys (HEA) are a recent class of alloys first prospected in 2004 by Cantor *et al* [1] as multi-component alloys containing five principal components near

*CONTACT Osman El-Atwani Email: osman@lanl.gov, Enrique Martinez Saez Email: enrique@clemson.edu

equiatomic ratios. Yeh *et al* [2,3] contributed to the term HEA for this type of alloy retaining a high configuration entropy of mixing at its near equiatomic solution phase. From the maximum entropy production principle [4], the high entropy promotes stability of random solutions rather than intermetallic phases and decompositions where configurational entropy is lower. Underlying these solution phases are regularly simple crystal structures. A majority of underlying phases in near equiatomic HEAs show face-centered cubic (FCC) or body-centered cubic (BCC) crystal structures. Although intermetallic phases may be desirable for unique applications [5], they are known to reduce ductility and disqualify them for applications as structural materials [6].

HEA differentiate from traditional materials by the high entropy, diffusion properties, and the large lattice-distortion effect. High hardness, yield strength, ductility, and fracture toughness in HEAs are often attributed to the severe lattice distortion [2,7,8] within the complex local chemistry of HEAs. Recently, a refractory high entropy alloy (RHEA) composed of W, Ta, Cr, V has been developed [9] exhibiting outstanding radiation resistance and thermal stability to grain growth under heavy ion irradiation at 1073 K. The W-Ta-Cr-V RHEA shows promising mechanical properties with a nanoindentation hardness of up to 14 GPa but inherently fails under tensile ductility. The presence of Hf in alloys has shown modification of the microstructure that improves low temperature ductility and high temperature creep resistance [10–12]. In addition, the valence electron concentration (VEC) is overall lowered when Hf is mixed with IV, V, and VI group elements. Studies of single-phase BCC RHEAs with VEC < 4.5 show the material is intrinsically ductile compared to intrinsically brittle at higher VEC [13,14]. Leong et al in Ref. [15] find from the electronic structure analysis that BCC structures present in base CoCrFeNi HEAs are stable with VECs ranging from 5.0 to 7.5

Computational models and simulations have been introduced, formulated, redesigned, and adapted to tackle the unique challenges of HEAs. In practice, solid solutions in FCC or BCC are desired, however there are large sets of compositions containing similar specie concentrations that have the potential to lead to phase decomposition. To analyze the enormous compositional space, techniques such as the cluster expansion (CE) method have been implemented alongside density functional theory (DFT) to predict the stability of random solutions [16,17]. CE has proven to be an efficient method for predicting the energy of a configuration as a function of composition. In the CE model, the energy of an alloy is denoted by a series of cluster functions. Put into terms of an energy expression the result is a generalized form of an Ising Hamiltonian that holds components of coupling parameters known as effective cluster interactions or ECIs [18]. In terms of first-principles computations, there are several approaches to compute the ECIs. The most often used technique is known as the structure inversion method (SIM) based on Connolly-Williams approximations [19]. The SIM is used here on energies of configurational structures computed by DFT. We develop a CE model based on DFT to probe the stability of disordered states after introducing Hf to the W-Ta-Cr-V RHEA.

2. Computational Methodology

DFT calculations are performed to inform the CE method. For the exchange and correlation, we use a generalized gradient approximation from Perdue-Burke-Erzenerhof (GGA-PBE) [20], with the projector augmented wave (PAW) pseudopotential method in the DFT software Vienna Ab-initio Simulation Package (VASP) [21,22]. Both the

semi-core p electron and magnetism contribution are not included in this study. We find the contribution from both do not significantly affect the calculations. The convergence criteria for energy was set to 10^{-5} eV per cell and force convergence criteria of 10^{-3} eV Å^{-1}. The Monkhorst-Pack mesh [23] spacing is such that it corresponds to a 14 × 14 × 14 k-point mesh of a two-atom body centered cubic cell at about 5000 k-points per atom. The plane-wave cutoff energy used was 400 eV.

In this study, the Alloy Theoretic Automated toolkit (ATAT) [24,25] package is used to generate a mapping from DFT's energies to CE's effective cluster interactions. A modified database of 58 initial structures for each binary subsystem was used following Ref. [26]. For ternary subsystems and following Ref. [27], the initial binary structures were subjected to symmetry rules and restrictions by number of nonequivalent positions (NEPs) to construct a resulting 94 ternary structures. For quaternary and quinary structures, a database from Ref. [28] was integrated and modified for W-Ta-Cr-V-Hf. In total, we have 1511 BCC structures focusing on quinary configurations and binaries, ternaries, and quaternaries subsystems of the W-Ta-Cr-V-Hf HEA.

The energy minimization during DFT relaxation are held at zero pressure and temperature while the volume and shape of the system are allowed to change. Of all possible structures to use in the fitting, a restriction is imposed to the volume change from a starting to ending structure. A cross-validation score of 13.62 meV is generated for this CE model using 60 two-body, 80 three-body and 55 four-body effective cluster interactions, meaning on average the CE model is able to predict energies for any given BCC structure within 14 meV per atom when compared to DFT energies. The reference energies for each principal element in BCC crystal structure are -9.511, -9.772, -11.862, -8.942, -13.011 eV per atom for Cr, Hf, Ta, V, W respectively as calculated by DFT of a 2 atom cell. The ground state energy of Hf is for the hexagonal-closed pack (HCP) structure, in which case the energy calculated from DFT is -9.951 eV per atom with the same VASP parametrization.

Monte Carlo simulations were performed using the Multicomponent Eazy Monte Carlo (MEMC) [29] code provided in the ATAT package. A disordered and randomized solution structure with composition $W_{.31}Ta_{.34}Cr_{.05}V_{.27}Hf_{.03}$ is used as initial input to generate 12 × 12 × 12 and 20 × 20 × 20 BCC unit cells with 3456 atoms and 16000 atoms, respectively. The simulation computes the enthalpy of mixing at each temperature step for a corresponding configuration in thermodynamic equilibrium within the temperature range. The start temperature for each simulation begins at 3000 K and reduced to 10 K with temperature step widths of 10 K. The start temperature is chosen such that a disordered configuration is near-guarantee after 2000 MC steps in thermalization and accumulation stages. This number of MC steps was used at every temperature in the present study.

The present work focuses on the enthalpy, entropy, and free energy of mixing along with the chemical short range order parameters (SROs) to determine the stability of the refractory W-Ta-Cr-V after Hf addition. The following methodology is similar to previously described CE studies [27,28], and is an extension of Ref. [28] to include Hf to the quaternary refractory HEA. Within a CE formalism the enthalpy of mixing is given by:

$$\Delta H_{\text{mix, CE}}(\vec{\sigma}) = \sum_{\omega} m_{\omega} J_{\omega} \langle \Gamma_{\omega'}(\vec{\sigma}) \rangle_{\omega} \tag{1}$$

with m_{ω}, J_{ω}, and $\langle \Gamma_{\omega'}(\vec{\sigma}) \rangle_{\omega}$ denoting the multiplicity of equivalent clusters ω, concentration-independent effective cluster interactions, and the average correlation

function given by products of the point functions of occupational variables $\vec{\sigma}$ over all clusters ω', respectively. The configurational entropy contribution to free energy of mixing is calculated using a thermodynamic integration method:

$$S_{\mathrm{conf}}(T) = \int_0^T \frac{C_{\mathrm{conf}}(T')}{T'} dT', \tag{2}$$

where the specific heat $C_{\mathrm{conf}}(T)$ is determined from the magnitude of the fluctuations in the enthalpy of mixing [30,31]

$$C_{\mathrm{conf}}(T) = \frac{\langle H_{\mathrm{mix}}(T)^2 \rangle - \langle H_{\mathrm{mix}}(T) \rangle^2}{T^2}. \tag{3}$$

The thermodynamic integration equations 1 and 2 can be used to calculate the free energy of mixing

$$G_{\mathrm{mix}} = H_{\mathrm{mix}} - TS_{\mathrm{conf}}. \tag{4}$$

3. Results and Discussion

The enthalpy of mixing for subsystems in the quinary HEA was calculated using DFT. The CE model was fit to the DFT data. With binary pairings similar to quaternary W-Ta-Cr-V HEAs and additional Hf parings consisting of Cr-Hf, Hf-Ta, Hf-V, and Hf-W pairs. Shown in Figure 1 are the enthalpies of mixing for Hf binaries. The total range of Hf concentration across each binary configuration are examined to determine atomic interactions. Positive values of enthalpy of mixing indicate a tendency of phase separation and negative values for ordering and formation of intermetallics. Enthalpy of mixing values near 0 eV per atom have the tendency of forming solid solutions.

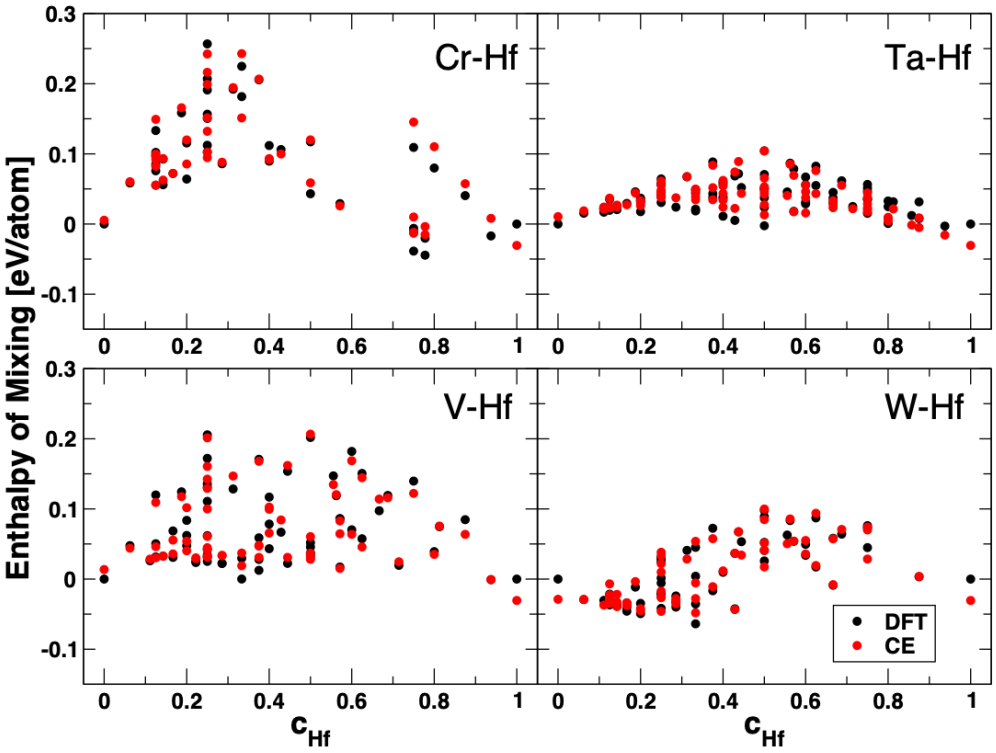

Figure 1. Enthalpy of mixing in eV per atom for Hf-binary pairs in the quinary W-Ta-Cr-V-Hf HEA from DFT and CE.

Pairings belonging solely to the quaternary HEA depict negative enthalpy values through all concentrations for the Cr-V and Ta-W pairs and positive values through all concentration for the Cr-W and Ta-V pairs, in agreement with Ref [28]. Shown in Figure 1 for the quinary HEA, Cr-Hf and Hf-W pairs contain negative enthalpies at the Hf-rich region while Hf-Ta and Hf-V pairs show positive values for their entire concentration range.

The addition of Hf proves to add complexity to the HEA as the stabilization of Hf-binaries may phase relax out of BCC to HCP at high Hf concentrations [32,33]. This is evident from Figure 1 in that at $c_{\mathrm{Hf}} = 1$ the model struggles to predict the energy obtained through DFT. Careful review of binary and ternary subsystems of this HEA was necessary to prevent invalid data represented in the model. Extensive studies on Hf alloys show significant ground state structures in the Laves C15 phase. Relevant to this study are the binaries cubic C15 $HfCr_2$ [34,35] and HfW_2 [35] displaying an enthalpy of formation lower than that of BCC. From DFT, $C11_b$ $HfCr_2$ BCC displays an enthalpy of formation of 102 meV per atom. The enthalpy of formation for C15 Laves structure of $HfCr_2$ gives -117 meV per atom from DFT calculations. BCC HfW_2 enthalpy of formation from DFT is -4.4 meV per atom as opposed to its Laves phase enthalpy of formation at -179 meV per atom. At lower temperatures, $HfCr_2$ would have a greater tendency to stabilize at the Laves phase than BCC, which would not be captured in the BCC quinary system CE model and the Monte Carlo simulations shown here. However, experiments at 300 K show predominantly a BCC phase.

As a product of the CE method, an *ab initio* based Hamiltonian containing effec-

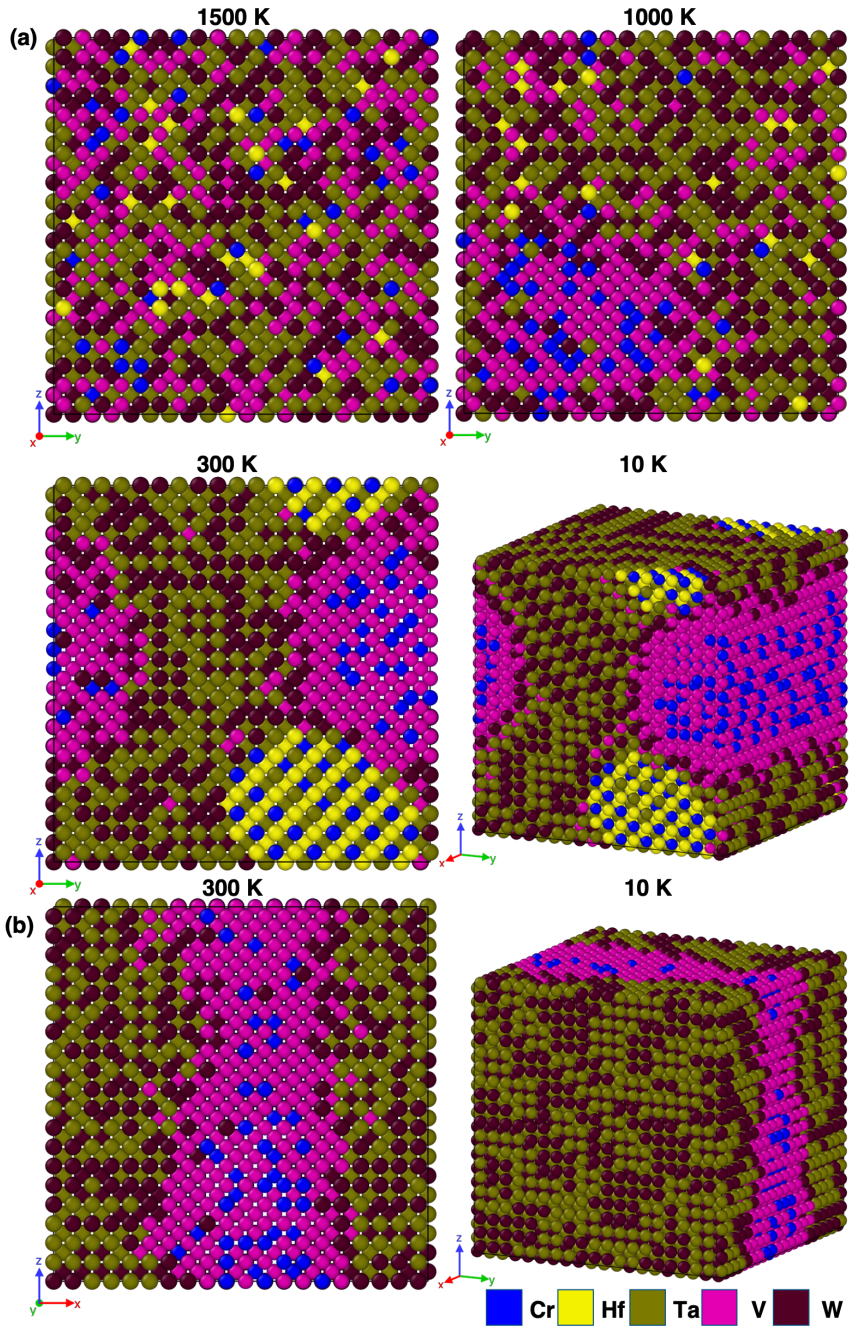

Figure 2. 16000 atom simulation cell of the (a) quinary $W_{.31}Ta_{.34}Cr_{.05}V_{.27}Hf_{.03}$ HEA at 1500 K, 1000 K, 300 K, and 10K and (b) quaternary $W_{.31}Ta_{.34}Cr_{.05}V_{.3}$ HEA at 300 K and 10 K.

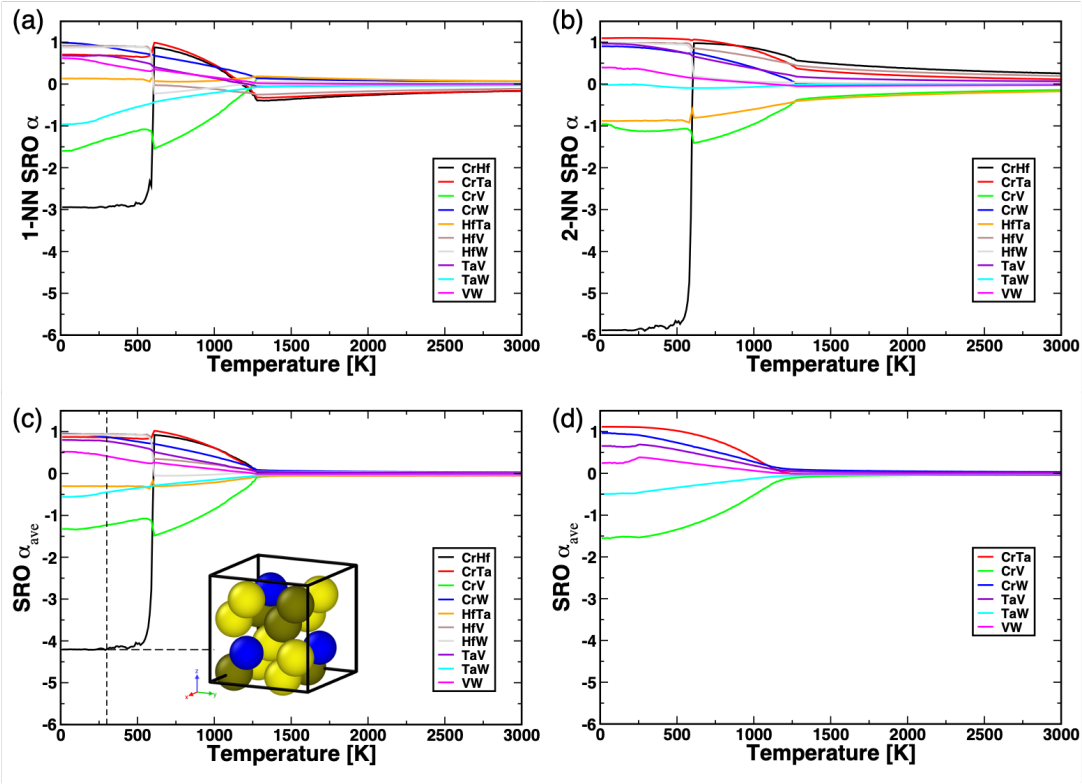

Figure 3. Chemical short-range ordering as a function of temperature for (a) the first and (b) second nearest neighbor (NN) SRO of the quinary HEA from 0 to 3000 K, (c) the quinary $W_{.31}Ta_{.34}Cr_{.05}V_{.27}Hf_{.03}$ HEA with an inset of a Cr-Hf-Ta cell at 300 K with atomic coloring equal to Figure 2 and (d) quaternary $W_{.31}Ta_{.34}Cr_{.05}V_{.30}$.

tive cluster interactions is utilized in Monte Carlo simulations. Figure 2a shows Monte Carlo snapshots of 16000 atom configurations at 1500 K, 1000 K, 300 K, and 10 K for a quinary HEA. Figure 2b shows MC snapshots at 300 K and 10 K for quaternary HEA of similar composition. For Figure 2a, at 1500 K the MC simulation finds random disordered solutions as a stable configuration. At 1000 K a transition from random configuration to phase separation with clustering of Cr and V is observed. The precipitates observed at 300 K and 10 K in Figure 2a are majorly composed of Cr-V with a second Cr-Hf-Ta precipitate attached to the side of the Cr-V region. The decrease in temperature leads to further ordering of the W-Ta pair. As opposed to the quaternary refractory HEA, Figure 2b, the quinary HEA contains two precipitate systems, one composed of a Cr-Hf-Ta subsystem and the familiar Cr-V cluster. From Figure 2, it is observed that an order-disorder transition occurs between 1000 to 1500 K temperature range and a second phase transition from order to phase separation occurs from 300 K to 1000 K.

Figures 3a and 3b show the Warren-Cowley SRO parameters for pair interactions in the quinary HEA for the first and second nearest neighbor shells given by

$$\alpha_n^{ij} = 1 - \frac{y_n^{ij}}{c_i c_j}, \tag{5}$$

where α_n^{ij}, y_n^{ij}, and c are the chemical short-range order parameter, probability of finding two atoms within n^{th} neighbors, and concentrations, respectively, for i and j distinct principal elements. Figures 3c and 3d present the average SRO from the first and second nearest neighbors for both the quinary and quaternary HEAs. The order-disorder transition temperature (ODTT) can also be analyzed through the SRO parameter. The analysis of the SRO parameters highlights the existence of two transitions, one around 1250 K from fully disorder to order/phase separation depending on the pair and another one around 620 K led by the transition of the Cr-Hf pair from phase separation to ordering. From these results we observe that Hf clearly adds complexity to the system with a new transition at around 620 K that affects all pairs in the system.

At low temperatures in Figure 3c, for all but Cr-Hf, Cr-V, Hf-Ta, and Ta-W pairs there are clear positive chemical ordering. The strength of the chemical ordering as shown by the SRO parameters can be, in part, explained from Equation 5. In this equation the SRO is inversely proportional to the product of concentrations, which are lowest among Cr and Hf. The trend in Figure 3c is suggestive of a disordering between all given pairs at 1250 K. At lower temperatures, the Cr-Hf pair switches from negative to positive at 620 K, indicative of a first order transition from order to phase separation. Around 620 K, there is a discontinuity in the SRO values led by the behavior of Hf. The shift in ordering of pairs is initiated with mixing of Cr-Hf in the solution, enabling Cr and Hf species to pair with other principal elements beyond this transition temperature. Before averaging, the Hf-Ta pair exhibits positive SRO between first nearest neighbors and negative SRO between second nearest neighbors, for an average close to zero.

Studies on HEA microstructure [36,37] have shown ductility enhancement attributed to SRO induced microstructures. Our CE model suggests precipitates from the SRO parameters shown in Figure 3. The inset in Figure 3c is a sketch of the Cr-Hf-Ta precipitate displayed in Figure 2 at 300 K. The 16-atom cell depicts 8 Hf atoms in a first neighbor shell with other surrounding ordered Cr, and Ta atoms. With low concentrations of Hf, SRO can be tuned as shown in the contrast between the quaternary and quinary HEA Figs. 3c and 3d.

The SRO for pairs that do not include Hf in the quinary HEA are similar to those observed in the quaternary [9]. Figure 3d shows a clear and strong negative chemical ordering in the quaternary system for Cr-V and Ta-W pairs, with the other pairs showing a separation tendency. The discontinuity observed at around 620 K in the SRO for the quinary is not present in the quaternary, highlighting the global effect of Hf in the behaviour of the alloy. The ordering does not fade until the SRO parameter of all pairs converges to zero, at around 1250 K.

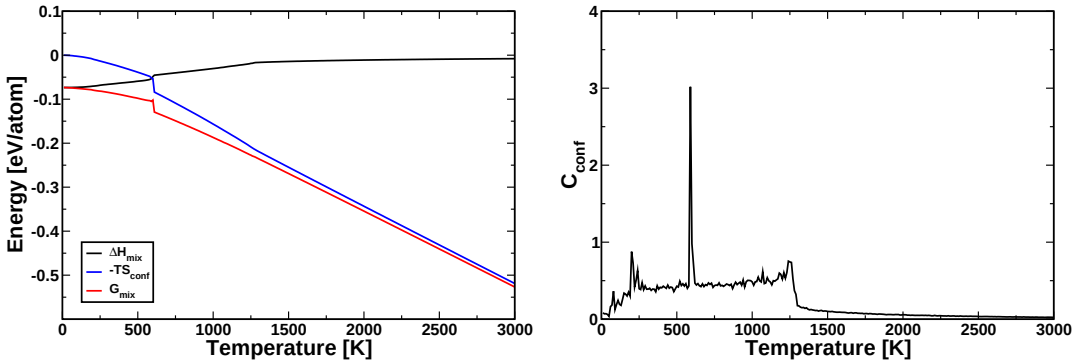

(a) (b)

Figure 4. (a) Enthalpy of mixing, configurational entropy, and free energy and (b) specific heat as a function of temperature of the quinary $W_{.31}Ta_{.34}Cr_{.05}V_{.27}Hf_{.03}$ HEA.

The enthalpy of mixing, configurational entropy, and free energy as a function of temperature are calculated from DFT-based Monte Carlo simulations following Eqs. 1, 2, and 4 and are shown in Figure 4a. The specific heat of the quinary HEA as a function of temperature is shown in Figure 4b as calculated by Equation 3. In Figure 4a, a discontinuity is observed in the enthalpy, entropy, and free energy curve at a temperature about 620 K and a change of slope at 1250 K noticeable for the enthalpy of mixing and entropy. The discontinuity can be attributed to the system phase transitioning. These results show the free energy exhibits a first order transition at 620 K with the Cr-Hf pairs disassociating and a second order transition at 1250 K with all pairs mixing into the HEA. Figure 4b shows a higher specific heat at lower temperatures, at which the system is short-range ordered. A discontinuity in the specific heat is observed at 620 K while above 1250 K the specific heat decreases coinciding with the disordered region. Another discontinuity is observed at about 200 K which can be associated with Ta-W pairs short-range ordering as observed at 10 K in Figure 2.

3.1. Experimental data

Figure 5a shows the results at room temperature of atom probe tomography (APT) for the quinary HEA with average concentrations of $W_{.31}Ta_{.34}Cr_{.05}V_{.27}Hf_{.03}$. The APT samples were fabricated using standard lift out and sharpening methods as described by Thompson et al. [38]. Briefly, wedges were lifted out, mounted on Si microtip array posts, sharpened using a 30 kV Ga+ ion beam, and cleaned using a 2 kV Ga+ ion beam. The APT experiment was run using a CAMECA LEAP 4000XHR in laser mode with a 30 K base temperature, 80-100 pJ laser energy, a 0.5 % detection rate, and a pulse repetition rate set to capture all elements in the mass spectra. The APT results were reconstructed and analyzed using CAMECA's interactive visualization and analysis software (IVAS 3.8).

From the APT, a layered structure is observed in the inset of Figure 5 and visualized as a concentration plot. The profile depicts 3 nm regions with high Ta and W concentrations and low Cr, Hf, and V concentrations and separated by 2 nm regions with elevated concentrations of Cr, Hf, and V and lower concentrations of Ta and W. The concentration plot of each element is gathered from a line scan of the APT up to

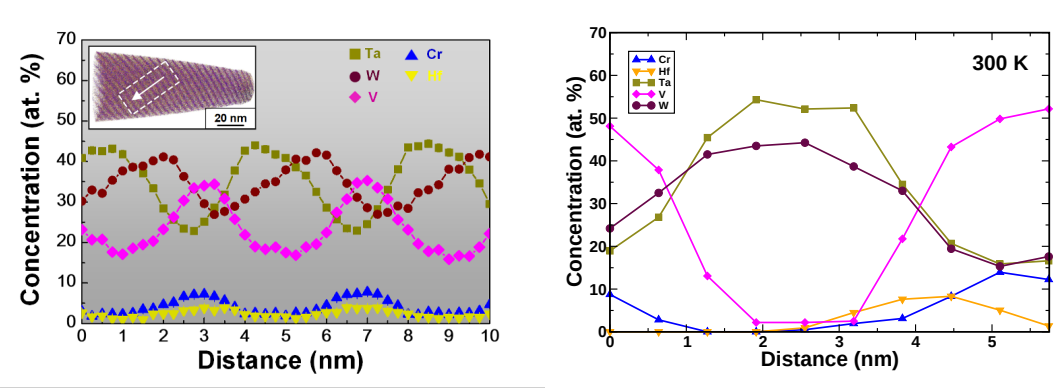

(a) (b)

Figure 5. (a) Concentration plot and APT image, in the inset, of $W_{.31}Ta_{.34}Cr_{.05}V_{.27}Hf_{.03}$ HEA and (b) concentration profile of from Monte Carlo simulation at 300 K.

a distance of 10 nm and compared with a simulation cell corresponding to side lengths of 5.7 nm.

Figure 5b shows a concentration plot gathered from Monte Carlo simulations at 300 K along the y-direction relative to the snapshots shown in Figure 2. We observe correlations between three elements, Cr, Hf, and V, and pairs Ta and W. The correlations shown in both Figures 5a and 5b are supported by the calculated SROs from our CE method, Figure 3, in that at temperatures below 620 K, Ta-W, Cr-Hf, and Cr-V pairs show negative SRO. Although V-Hf pairs do not directly report a negative SRO in any case shown in Figure 3, the strength of interaction between Cr-Hf is sufficiently strong to show correlations with V and Hf in experiments and Monte Carlo concentration plots. This indirect correlation explains the observance of Cr-Hf-Ta precipitates near Cr-V precipitates as in Figure 2.

Figure 5a displays shifted peaks between W and Ta that are not reflected in the CE model. Further investigations are required to explain the discrepancies between the two concentration profiles, experimental and from MC simulations.

4. Conclusion

We have developed a design methodology to study the thermal stability and concentration landscape of W-Ta-Cr-V RHEA with the addition of Hf. The model developed for the quinary BCC Cr-Hf-Ta-V-W system from the DFT-based CE method shows a cross validation score of 13.62 meV. We find for the concentration explored, $W_{.31}Ta_{.34}Cr_{.05}V_{.27}Hf_{.03}$, the addition of Hf increases the complexity of SRO parameters and pairings between each principal element as compared to the quaternary RHEA. Strong negative chemical ordering is displayed among Cr-Hf, Cr-V, and Ta-W pairs within the temperature range from 0 to 1250 K. The ODTT found analyzing the enthalpy, entropy, and free energy curves are at around 620 K and 1250 K. At 620 K, the SRO analysis shows Cr-Hf pairs mix into the HEA, while Cr-V precipitates remain stable until 1250 K.

The CE model demonstrated here is easily extendable for an addition or substitution of principal elements. Within the 1511 BCC structures, binary, ternary, and quaternary subsystems are carefully examined and included to accurately reflect the inclusion of

Hf from previous iterations of RHEA CE models. In addition, the CE model is readily available to survey the concentration landscape found in HEAs.

Finally, the CE results show good agreement with experiments. Given the same concentration, both CE and experiments display similar trends between species. From APT and MC simulations, both concentration profiles depict regions of correlation between Ta-W and a secondary region with correlations between Cr-Hf-V. The agreement between model and experiment give confidence to explore further concentrations of this complex rHEA and systematically probe thermodynamic effects of additional Hf in W-Ta-Cr-V rHEA.

5. Acknowledgments

A.A. and O.E. acknowledge support from the LDRD-ERC program at Los Alamos National Laboratory. E.M. acknowledges support by the National Science Foundation EPSCoR Program under NSF Award # OIA-1655740. Any opinions, findings and conclusions or recommendations expressed in this material are those of the author(s) and do not necessarily reflect those of the National Science Foundation. DNM, JSW and DS work has been carried out within the framework of the EUROfusion Consortium, funded by the European Union via the Euratom Research and Training Programme (Grant Agreement No 101052200 — EUROfusion). Views and opinions expressed are however those of the author(s) only and do not necessarily reflect those of the European Union or the European Commission. Neither the European Union nor the European Commission can be held responsible for them. DNM also acknowledges funding from the RCUK Energy Programme Grant No. EP/W006839/1. The work at WUT has been carried out as a part of an international project co-financed from the funds of the program of the Polish Minister of Science and Higher Education entitled "PMW" in 2019; Agreement No. 5018 / H2020-Euratom / 2019/2. DNM and JSW would like to thank the support from high-performing computing facility MARCONI (Bologna, Italy) provided by EUROfusion.

References

[1] Brain Cantor, ITH Chang, P Knight, and AJB Vincent. Microstructural development in equiatomic multicomponent alloys. *Materials Science and Engineering: A*, 375:213–218, 2004.

[2] J.-W. Yeh, S.-K. Chen, S.-J. Lin, J.-Y. Gan, T.-S. Chin, T.-T. Shun, C.-H. Tsau, and S.-Y. Chang. Nanostructured high-entropy alloys with multiple principal elements: Novel alloy design concepts and outcomes. *Advanced Engineering Materials*, 6(5):299–303, 2004.

[3] Jien-Wei Yeh. Recent progress in high-entropy alloys. *Annales de Chimie. Science des Materiaux (Paris)*, 31(6):633–648, 2006.

[4] L.M. Martyushev and V.D. Seleznev. Maximum entropy production principle in physics, chemistry and biology. *Physics Reports*, 426(1):1–45, 2006.

[5] M. Yamaguchi, H. Inui, and K. Ito. High-temperature structural intermetallics. *Acta Materialia*, 48(1):307–322, 2000.

[6] Z.B. Jiao, J.H. Luan, and C.T. Liu. Strategies for improving ductility of ordered intermetallics. *Progress in Natural Science: Materials International*, 26(1):1–12, 2016.

[7] Y. J. Zhou, Y. Zhang, Y. L. Wang, and G. L. Chen. Solid solution alloys of alcocrfenitix with excellent room-temperature mechanical properties. *Applied Physics Letters*, 90(18):181904, 2007.

[8] E.P. George, W.A. Curtin, and C.C. Tasan. High entropy alloys: A focused review of mechanical properties and deformation mechanisms. *Acta Materialia*, 188:435–474, 2020.

[9] O. El-Atwani, N. Li, M. Li, A. Devaraj, J. K. S. Baldwin, M. M. Schneider, D. Sobieraj, J. S. Wróbel, D. Nguyen-Manh, S. A. Maloy, and E. Martinez. Outstanding radiation resistance of tungsten-based high-entropy alloys. *Science Advances*, 5(3), 2019.

[10] P. S. Kotval, J. D. Venables, and R. W. Calder. The role of hafnium in modifying the microstructure of cast nickel-base superalloys. *Metallurgical and Materials Transactions B*, 3(2):457–462, 1972.

[11] M. Manjula and M. Sundareswari. Effect of hafnium ternary addition on ductility of aerospace material rh3ta – a theoretical study. *Materials Today: Proceedings*, 3(9, Part B):2991–2996, 2016. Advances in Refractory and Reactive Metals and Alloys (ARRMA 2016).

[12] Shao-Ping Wang, Evan Ma, and Jian Xu. New ternary equi-atomic refractory medium-entropy alloys with tensile ductility: Hafnium versus titanium into nbta-based solution. *Intermetallics*, 107:15–23, 2019.

[13] Saad Sheikh, Samrand Shafeie, Qiang Hu, Johan Ahlström, Christer Persson, Jaroslav Veselý, Jiří Zýka, Uta Klement, and Sheng Guo. Alloy design for intrinsically ductile refractory high-entropy alloys. *Journal of Applied Physics*, 120(16):164902, 2016.

[14] V. Soni, O. N. Senkov, B. Gwalani, D. B. Miracle, and R. Banerjee. Microstructural design for improving ductility of an initially brittle refractory high entropy alloy. *Scientific Reports*, 8(1):8816, 2018.

[15] Zhaoyuan Leong, Jan S. Wróbel, Sergei L. Dudarev, Russell Goodall, Iain Todd, and Duc Nguyen-Manh. The effect of electronic structure on the phases present in high entropy alloys. *Scientific Reports*, 7(1):39803, 2017.

[16] S. Müller, M. Stöhr, and O. Wieckhorst. Structure and stability of binary alloy surfaces: Segregation, relaxation, and ordering from first-principles calculations. *Applied Physics A*, 82(3):415–419, 2006.

[17] Gus L. W. Hart, Volker Blum, Michael J. Walorski, and Alex Zunger. Evolutionary approach for determining first-principles hamiltonians. *Nature Materials*, 4(5):391—394, 2005.

[18] J.M. Sanchez, F. Ducastelle, and D. Gratias. Generalized cluster description of multicomponent systems. *Physica A: Statistical Mechanics and its Applications*, 128(1):334–350, 1984.

[19] J. W. D. Connolly and A. R. Williams. Density-functional theory applied to phase transformations in transition-metal alloys. *Phys. Rev. B*, 27:5169–5172, Apr 1983.

[20] John P. Perdew, Kieron Burke, and Matthias Ernzerhof. Generalized gradient approximation made simple. *Phys. Rev. Lett.*, 77:3865–3868, Oct 1996.

[21] G. Kresse and J. Hafner. Ab initio molecular dynamics for liquid metals. *Phys. Rev. B*, 47:558–561, Jan 1993.

[22] G. Kresse and J. Furthmüller. Efficient iterative schemes for ab initio total-energy calculations using a plane-wave basis set. *Phys. Rev. B*, 54:11169–11186, Oct 1996.

[23] Hendrik J. Monkhorst and James D. Pack. Special points for brillouin-zone integrations. *Phys. Rev. B*, 13:5188–5192, Jun 1976.

[24] A. van de Walle, M. Asta, and G. Ceder. The alloy theoretic automated toolkit: A user guide. *Calphad*, 26(4):539–553, 2002.

[25] Axel van de Walle. Multicomponent multisublattice alloys, nonconfigurational entropy and other additions to the alloy theoretic automated toolkit. *Calphad*, 33(2):266–278, 2009. Tools for Computational Thermodynamics.

[26] D. Nguyen-Manh, M. Yu. Lavrentiev, and S. L. Dudarev. Magnetic origin of nano-clustering and point defect interaction in fe–cr alloys: an ab-initio study. *Journal of Computer-Aided Materials Design*, 14(1):159–169, 2007.

[27] Jan S. Wróbel, Duc Nguyen-Manh, Mikhail Yu. Lavrentiev, Marek Muzyk, and Sergei L. Dudarev. Phase stability of ternary fcc and bcc fe-cr-ni alloys. *Phys. Rev. B*, 91:024108, Jan 2015.

[28] Damian Sobieraj, Jan S. Wróbel, Tomasz Rygier, Krzysztof J. Kurzydłowski, Osman El Atwani, Arun Devaraj, Enrique Martinez Saez, and Duc Nguyen-Manh. Chemical short-range order in derivative cr–ta–ti–v–w high entropy alloys from the first-principles thermodynamic study. *Phys. Chem. Chem. Phys.*, 22:23929–23951, 2020.

[29] A van de Walle and M Asta. Self-driven lattice-model monte carlo simulations of alloy thermodynamic properties and phase diagrams. *Modelling and Simulation in Materials Science and Engineering*, 10(5):521–538, jul 2002.

[30] M. E. J. Newman and G. T. Barkema. *Monte Carlo Methods in Statistical Physics*. Clarendon Press, 1999.

[31] M. Y. Lavrentiev, S. L. Dudarev, and D. Nguyen-Manh. Magnetic cluster expansion simulations of fecr alloys. *Journal of Nuclear Materials*, 386-388:22–25, 2009.

[32] D.R. Holmes. Corrosion of Hafnium and Hafnium Alloys. In *Corrosion: Materials*. ASM International, 01 2005.

[33] Ralph H. Nielsen and Updated by Staff. *Hafnium and Hafnium Compounds*, pages 1–19. John Wiley & Sons, Ltd, 2013.

[34] Xing-Qiu Chen, W. Wolf, R. Podloucky, and P. Rogl. Ab initio study of ground-state properties of the laves phase compounds $ticr_2$, $zrcr_2$, and $hfcr_2$. *Phys. Rev. B*, 71:174101, May 2005.

[35] Ohad Levy, Gus L.W. Hart, and Stefano Curtarolo. Hafnium binary alloys from experiments and first principles. *Acta Materialia*, 58(8):2887–2897, 2010.

[36] Qingqing Ding, Yin Zhang, Xiao Chen, Xiaoqian Fu, Dengke Chen, Sijing Chen, Lin Gu, Fei Wei, Hongbin Bei, Yanfei Gao, Minru Wen, Jixue Li, Ze Zhang, Ting Zhu, Robert O. Ritchie, and Qian Yu. Tuning element distribution, structure and properties by composition in high-entropy alloys. *Nature*, 574(7777):223–227, 2019.

[37] Shuai Chen, Zachary H. Aitken, Subrahmanyam Pattamatta, Zhaoxuan Wu, Zhi Gen Yu, David J. Srolovitz, Peter K. Liaw, and Yong-Wei Zhang. Simultaneously enhancing the ultimate strength and ductility of high-entropy alloys via short-range ordering. *Nature Communications*, 12(1):4953, 2021.

[38] K Thompson, D Lawrence, D J Larson, J D Olson, T F Kelly, and B Gorman. In situ site-specific specimen preparation for atom probe tomography. *Ultramicroscopy*, 107(2-3):131–139, Feb-Mar 2007.